THE JOURNAL OF BIOLOGICAL CHEMISTRY VOL. 285, NO. 8, pp. 5917–5930, February 19, 2010

Ligand-bound Structures Provide Atomic Snapshots for the Catalytic Mechanism of D-Amino Acid Deacylase*[S]

Received for publication, July 6, 2009, and in revised form, November 12, 2009 Published, JBC Papers in Press, December 9, 2009, DOI 10.1074/jbc.M109.038562

Tarun Kumar Bhatt[‡1,2], **Manickam Yogavel**[‡1], **Sandra Wydau**[§¶], **Ritu Berwal**[‡], **and Amit Sharma**[‡2,3]

From the [‡]*Structural and Computational Biology Group, International Centre for Genetic Engineering and Biotechnology (ICGEB), Aruna Asaf Ali Road, New Delhi, 110067, India and the* [§]*Laboratoire de Biochimie and* [¶]*CNRS UMR7654, Laboratoire de Biochimie, Ecole Polytechnique, F-91128 Palaiseau Cedex, France*

D-tyrosyl-tRNA^{Tyr} deacylase (DTD) is an editing enzyme that removes D-amino acids from mischarged tRNAs. We describe an in-depth analysis of the malaria parasite *Plasmodium falciparum* DTD here. Our data provide structural insights into DTD complexes with adenosine and D-amino acids. Bound adenosine is proximal to the DTD catalysis site, and it represents the authentic terminal adenosine of charged tRNA. DTD-bound D-amino acids cluster at three different subsites within the overall active site pocket. These subsites, called transition, active, and exit subsites allow docking, re-orientation, chiral selection, catalysis, and exit of the free D-amino acid from DTD. Our studies reveal variable modes of D-amino acid recognition by DTDs, suggesting an inherent plasticity that can accommodate all D-amino acids. An in-depth analysis of native, ADP-bound, and D-amino acid-complexed DTD structures provide the first atomic snapshots of ligand recognition and subsequent catalysis by this enzyme family. We have mapped sites for the deacylation reaction and mark possible routes for entry and egress of all substrates and products. We have also performed structure-based inhibitor discovery and tested lead compounds against the malaria parasite *P. falciparum* using growth inhibition assays. Our studies provide a comprehensive structural basis for the catalytic mechanism of DTD enzymes and have implications for inhibition of this enzyme in *P. falciparum* as a route to inhibiting the parasite.

Aminoacyl-tRNA synthetases (aaRSs) transfer L-amino acids to their cognate tRNA and are essential in the protein translation process. However, at times aaRS enzymes can also attach D-amino acids to tRNA, and this mistake can be toxic to growing cells. Tyrosyl-tRNA synthetases from *Escherichia coli* and *Bacillus subtilis* (1, 2), tyrosyl-tRNA synthetases from *Saccharomyces cerevisiae* (3) and tryptophanyl/aspartyl-tRNA synthetases from *S. cerevisiae* (4) can transfer D-forms of their cognate amino acids onto relevant tRNAs. To avoid introduction of D-amino acids in the translation machinery, almost all cells have editing domains like D-tyrosyl-tRNA^{Tyr} deacylase (DTD).[4] This enzyme cleaves the bond between D-amino acids and tRNA (Fig. 1*A*) and is encoded by the *dtd* gene in *E. coli* (5) and by the *dtd1* gene in *S. cerevisiae* (3). Homologs of *dtd*/*dtd1* genes are found in many genomes (*S. cerevisiae*, *Caenorhabditis elegans*, mouse, human (5), but not in archaea (4). However, another *dtd2* (previously named *GEK1*) gene homologous to *dtd*/*dtd1* is found in archaea and plants (6, 7). DTD enzymes exhibit broad specificity toward various D-amino acid-charged tRNAs (D-aa-tRNA) and are essentially inactive toward L-aa-tRNAs (2). Human DTD, also called DUE-B, has a long C-terminal extension and seems to be involved in D-amino acid resistance by deacylating D-aa-tRNAs during tRNA export (8).

Plasmodium parasites are causative agents of malaria, which affects >500 million people and claims ~2 million lives annually (9). In the *Plasmodium falciparum* genome, there are no sequence homologs for D-amino acid oxidase and D-Ser racemase, but a single copy of the *dtd* gene is present. PfDTD may therefore be responsible for detoxification of D-amino acids in this parasite. The molecular weight of PfDTD is ~20 kDa, and the sequence identity between PfDTD and its human homolog (HsDUE-B) is ~35%.

Native DTD structures have been reported from *Aquifex aeolicus* (AaDTD: PDB code 2DBO), *E. coli* (EcDTD: PDB code 1JKE, Ref. 10), *Haemophilus influenza* (HiDTD: PDB code 1J7G, Ref. 11), *Homo sapiens* (HsDTD: PDB code 2OKV, Ref. 12), and *Leishmania major* (LmDTD: PDB code 1TC5). A catalytic mechanism has also been proposed on the basis of mutagenesis and tRNA modeling onto DTDs (11, 12). However, to date, there are no DTD-ligand complex

* This work has been conducted as part of the MEPHITIS project and was supported in part by the European Commission (Grant Agreement HEALTH-F3-2009-223024).

⌘ *Author's Choice*—Final version full access.

The atomic coordinates and structure factors (codes 3KNF, 3KNP, 3KO3, 3KO4, 3KO5, 3KO7, 3KO9, 3KOB, 3KOC, and 3KOD) have been deposited in the Protein Data Bank, Research Collaboratory for Structural Bioinformatics, Rutgers University, New Brunswick, NJ (http://www.rcsb.org/).

[S] The on-line version of this article (available at http://www.jbc.org) contains supplemental Figs. S1–S3 and Table S1.

[1] Both authors contributed equally to this work.

[2] Supported by grants from the Dept. of Biotechnology, Government of India.

[3] To whom correspondence should be addressed. Tel.: 91-11-26741731; E-mail: amit.icgeb@gmail.com.

[4] The abbreviations used are: DTD, D-tyrosyl-tRNA^{Tyr} deacylase; PfDTD, *P. falciparum* DTD; AaDTD, *A. aeolicus* DTD; EcDTD, *E. coli* DTD; HiDTD, *H. influenzae* DTD; HsDTD, *H. sapiens* DTD; A3S, seryl-3′-aminoadenosine; A3Y, tyrosyl-3′-aminoadenosine; DAPI, 4′,6-diamidino-2-phenylindole; NTA, nitrilotriacetic acid; PEG, polyethylene glycol; MES, 4-morpholineethanesulfonic acid; PBS, phosphate-buffered saline; r.m.s.d., root mean-square deviation.

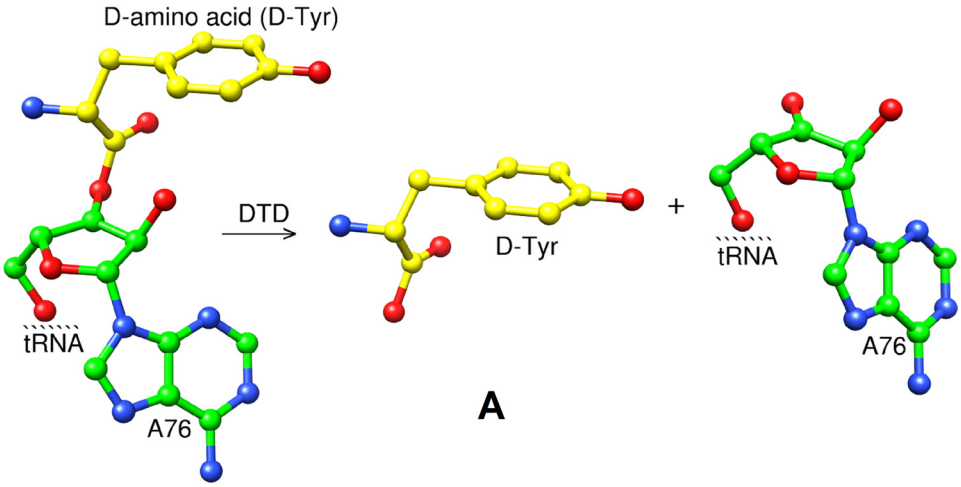

A

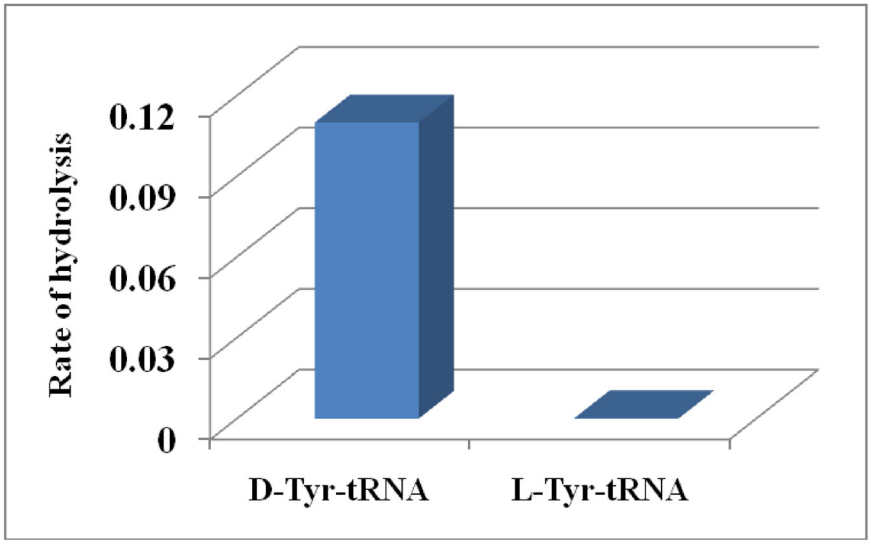

B

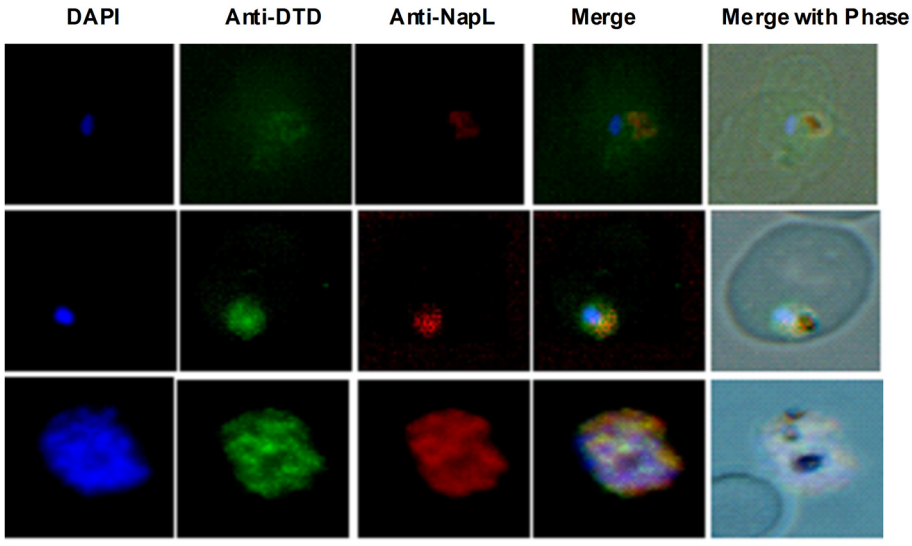

C

FIGURE 1. **Expression and activity of PfDTD.** *A*, schematic representation of deacylation process. *B*, enzyme activity and selectivity of PfDTD. Rate of L-Tyr-tRNA deacylation was significantly lower than of D-Tyr-tRNA hydrolysis. *C*, localization of PfDTD in different intra-erythrocytic stages of *P. falciparum* by immunofluorescence staining, Ring stage (*R*), trophozoite stage (*T*), and schizont stage (*S*) are shown. In each panel are shown: (*i*) image of cell stained with DAPI (*blue*), (*ii*) anti-PfDTD antibodies, (*iii*) anti-PfNapL antibodies, (*iv*) merged image, (*v*) merge with phase contrast.

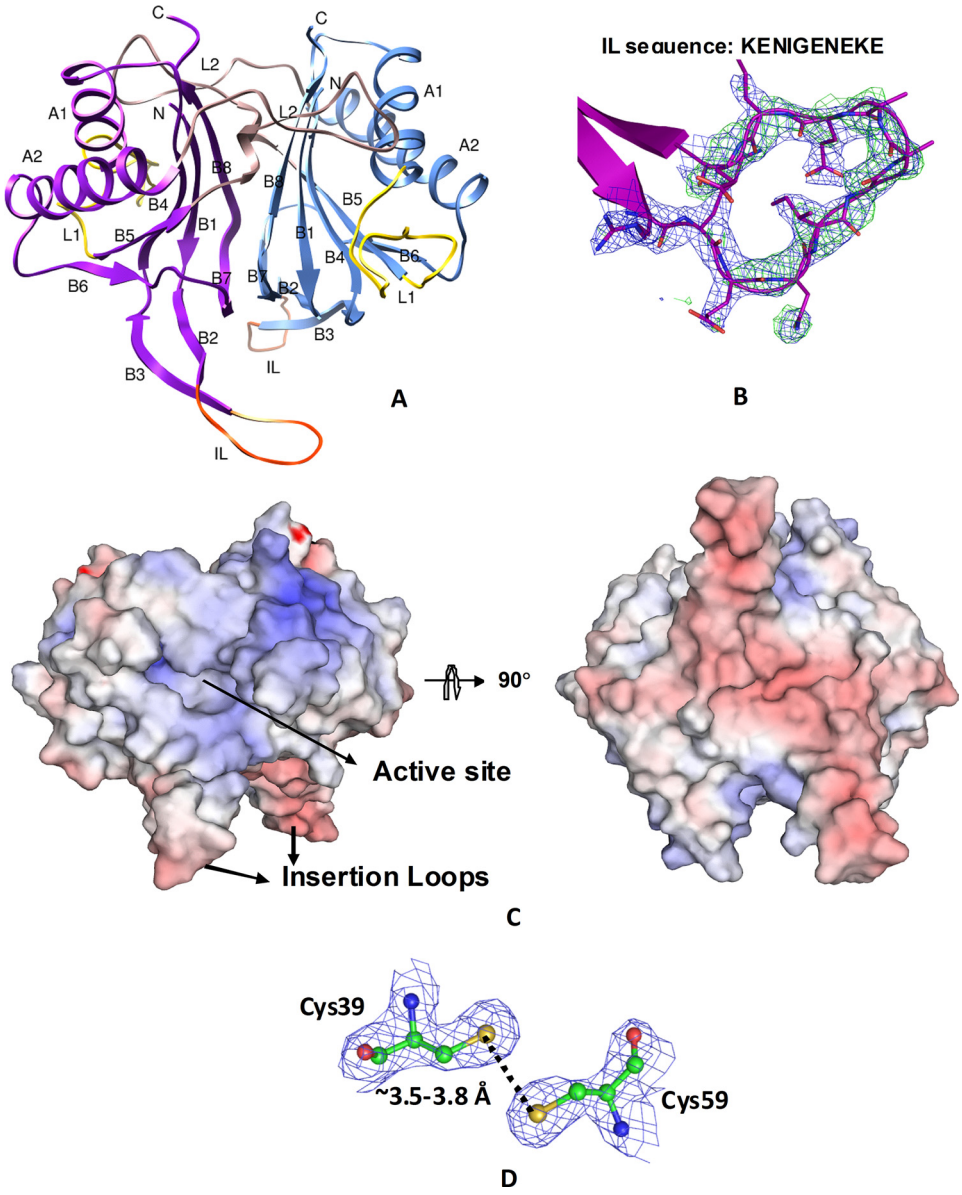

FIGURE 2. **Structure of PfDTD.** *A*, 2-fold-related dimeric molecules A and B are colored in *cornflower blue* and *purple*, respectively. Each monomer contains eight β-strands (B1–B8), two α-helices (A1 and A2), and three long loops (IL, L1, and L2). The low complexity insertion loop IL residues 17–26, loop L1 residues 55–65, and loop L2 residues 90–110 are highlighted in *orange*, *yellow*, and *brown*, respectively. The N and C termini are marked. *B*, ordered insertion loop (*IL*) in PfDTD-D-Lys complex structure. Difference Fourier (Fo-Fc) and final 2Fo-Fc maps are contoured at 2.5 and 1.0σ levels, respectively. *C*, orthogonal views showing electrostatic potential at the molecular surface of the PfDTD dimer. The orientation of the dimer is similar to the one shown in *A*. The electrostatic surface is displayed as a color gradient in *red* (electronegative, ≤ -12 kTe^{-1}) and *blue* (electropositive, ≥ 12 kTe^{-1}). *D*, view of reduced thiols in PfDTD. The final 2Fo-Fc map is contoured at the 2.5σ level.

structures known from any organism. Here, we report a whole set of crystal structures of DTD from *P. falciparum* complexed with adenosine and various D-amino acids. The crystal structures of native, ADP-bound, and D-amino acid-complexed PfDTDs provide key insights into the binding and recognition modes for various ligands. Based on the high resolution structures of PfDTD, we have also performed *in silico* inhibitor screening and present data for four compounds that inhibit parasite growth. We believe that our analysis not only provides a structural basis for the catalytic mechanism for this family of editing enzymes, but also highlights a possible new focus for the development of specific antimalarials.

EXPERIMENTAL PROCEDURES

Expression of PfDTD—The *dtd* gene from *P. falciparum* was PCR amplified and cloned between NcoI and KpnI restriction sites in modified pET28a vector, and PfDTD was expressed in fusion with histidine tag. *E. coli* B834 (DE3) cells were transformed with pET28DTD plasmid and grown at 37 °C in a culture medium (LB broth, USB). Culture was induced with isopropyl 1-thio-D-galactopyranoside (0.5 mM at OD of 0.6), and growth was continued for 5 h at 37 °C. The bacterial cell pellet was suspended in Ni-NTA buffer (50 mM NaH_2PO_4, 300 mM NaCl, 20 mM imidazole, pH 7.3) supplemented with lysozyme (100 μg ml^{-1}) and protease inhibitor mixture. Cells were sonicated and centrifuged at 14,000 rpm. The cleared supernatant was passed through Ni-NTA beads (Qiagen), which were then washed with Ni-NTA buffer to remove impurities, and protein was eluted with increasing concentration of imidazole (up to 500 mM). PfDTD protein was further purified via Superdex S-75 gel filtration chromatography (Amersham Biosciences). Purified PfDTD was concentrated using a 10 kDa Centricon (Viva Biosciences) and was buffer exchanged into crystallization buffer (25 mM Tris-HCl, pH 7.3, 100 mM NaCl, and 0.02% NaN_3).

Assay of D-Tyr-tRNA^{Tyr} Deacylase Activity—D-[^{3}H] and L-[^{14}C]Tyr-tRNA^{Tyr} were prepared as described previously (6). D-Tyr-tRNA^{Tyr} hydrolysis was followed for 5 min at 28 °C, in 100-μl assays containing: 20 mM Tris-HCl, pH 7.8, 3 mM $MgCl_2$, 100 nM D-[^{3}H]Tyr-tRNA, and 50 μg ml^{-1} bovine serum albumin. Prior to its addition to the assay, the enzyme was diluted in 20 mM Tris-HCl, pH 7.8, containing 200 μg ml^{-1} bovine serum albumin to obtain 80–400 pM of PfDTD in the test. The reaction was quenched by the addition of 340 μl of ethanol, 14 μl of sodium acetate 3 M (pH 4.8), and 20 μl of carrier RNA from yeast at 4 mg/ml. Samples were centrifuged (20 min, 20,600 $\times$ *g*, 4 °C), and radioactivity in the supernatant was measured by scintilla-

```
PfDTD   ARVVIQRVKGAILSVRKENIGENEKELEIISEIKNGLICFLGIHKNDTWE  50
HiDTD   MIALIQRVSQAKVDVK..........GETIGKIGKGLLVLLGVEKEDNRE  40
EcDTD   MIALIQRVTRASVTVE..........GEVTGEIGAGLLVLLGVEKDDDEQ  40
AaDTD   MRAVIQRVKKSWVEVD..........GKVVGSINEGLNVFLGVRKGDTEE  40
HsDTD   MKAVVQRVTRASVTVG..........GEQISAIGRGICVLLGISLEDTQK  40
          .::***. : : *             :  . *  *:  :**:   *  :

PfDTD   DALYIIRKCLNLRLWNN.DNK.TWDKNVKDLNYELLIVSQFTLFGNTKKG  98
HiDTD   KADKLAEKVLNYRIFSDE.N.DKMNLNVQQAQGELLIVSQFTLAADTQKG  88
EcDTD   KANRLCERVLGYRIFSDAE..GKMNLNVQQAGGSVLVVSQFTLAADTERG  88
AaDTD   DIEKLVNKILNLRIFED.ERG.KFQYSVLDIKGEILVVSQFTLYANVKKG  88
HsDTD   ELEHMVRKILNLRVFEDESGK.HWSKSVMDKQYEILCVSQFTLQ.CVLKG  88
        .   : .: *. *:: .:       . .* :   .:* ******   . :*

PfDTD   NKPDFHLAKEPNEALIFYNKIIDEFKKQYNDD.KIKIGKFGNYMNIDVTN 147
HiDTD   LRPSFSKGASPALANELYEYFIQKCAE.K...LPVSTGQFAADMQVSLTN 134
EcDTD   MRPSFSKGASPDRAEALYDYFVERCRQQ.E..MNTQTGRFAADMQVSLVN 135
AaDTD   RRPSFEEAEEPKRAKELYEKFVDKIKE.SG..LKVETGIFGAMMDVFIEN 135
HsDTD   NKPDFHLAMPTEQAEGFYNSFLEQLRKTYRPE.LIKDGKFGAYMQVHIQN 137
         :*.*  .  .  *  :*: :::.  :        . * *.  *:: : *

PfDTD   DGPVTIYIDTHDINLNK 164
HiDTD   DGPVTFWLNV....... 144
EcDTD   DGPVTFWLQV....... 145
AaDTD   WGPVTIIIDSREI.... 148
HsDTD   DGPVTIELESPA..... 149
         ****: ::
```

A

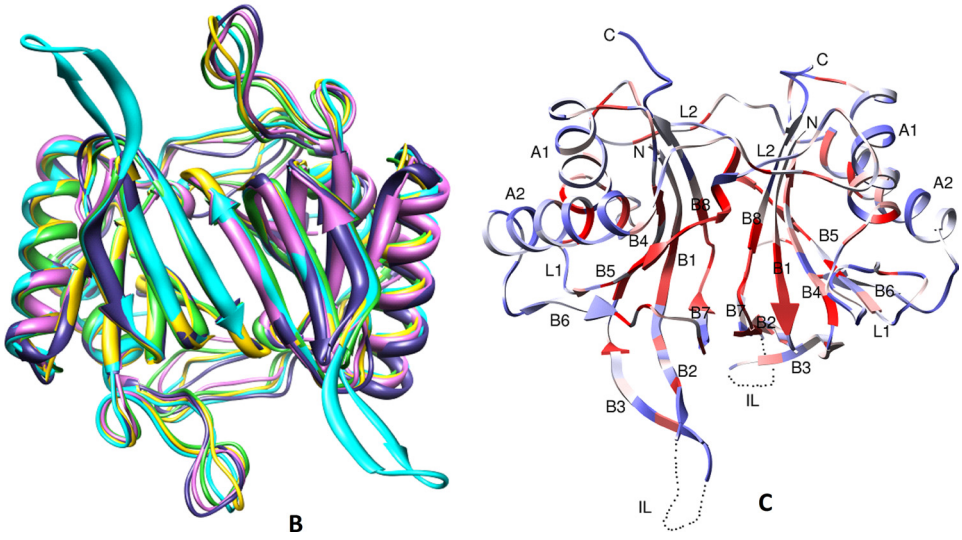

FIGURE 3. **Sequence conservation in DTDs.** *A*, structure-based sequence alignment of DTDs. Proteins are: *P. falciparum*, *A. aeolicus*, *E. coli*, *H. influenzae,* and *H. sapiens* (also known as the DNA-unwinding element-binding protein, DUEB). Identical/well conserved residues, conserved residues, and semi-conserved residues are marked with *asterisks*, *semicolons*, and *dots*, respectively. The two conserved active site motifs (*blue*), tRNA recognition residues (*green*), and 3′-end of tRNA and D-amino acid binding residues (*red*) are *highlighted*. *B*, superimposition of crystal structures of PfDTD (*cyan*), HsDTD (*purple*), AaDTD (*yellow*), EcDTD (*pink*), and HiDTD (*green*). *C*, residue conservation in DTDs is shown as a schematic diagram. Identical, well-conserved, semi-conserved, and weakly conserved residues are rendered in *red*, *pink*, *gray*, and *blue*, respectively.

tion counting. L-[^{14}C]Tyr-tRNA^{Tyr} hydrolysis was measured under the same conditions, except that the enzyme concentration was increased up to 400 nM. The enzyme concentration was based on an extinction coefficient of 25,565 M^{-1} cm^{-1}.

Immunofluorescence Assays—These were done essentially as described by Winter *et al.* (13) but with slight modifications. The asynchronous parasite pellet was washed twice in PBS, smeared onto a coverslip, and air dried. The smears were fixed in 1% formaldehyde in PBS for 30 min at room temperature and then rinsed in wash buffer (0.5% fetal bovine serum, 0.5% normal goat serum, 0.05% saponin) followed by blocking in PBS solution containing 5% skimmed milk powder, 5% goat serum, and 0.1% saponin. After washing, the coverslip were incubated with a mixture of affinity-purified rabbit anti-PfNapL antibodies (1:1000 dilution) and affinity-purified mouse anti-PfDTD antibody (1:1000 dilution) at room temperature with gentle shaking for 1 h. The coverslip was washed and incubated with a mixture of anti-rabbit antibody (1:500 dilution) conjugated to Alexa Fluor 594 (Molecular Probes) and anti-mouse antibody (1:500 dilution) conjugated to Alexa Fluor 488 (Molecular Probes) for 1 h at room temperature. Nuclei were stained by incubating the coverslip in PBS containing 3 μg/ml DAPI stain (Molecular Probes) for 5 min at room temperature, and after washing, the coverslip was mounted on slides with Antifade (Molecular Probes). Fluorescence microscopy was performed on a Nikon eclipse TE2000-U microscope.

Crystallization and Data Collection—Crystallization of PfDTD was carried out at room temperature using the hanging-drop vapor-diffusion method by mixing 1 μl of protein solution (5–10 mg ml^{-1}) with 1 μl of reservoir solution, and this was equilibrated against 200 μl of well liquor. Plate-shaped crystals were obtained using 0.1 M MES pH 6.2–6.8 and 25–30% PEG3350 or 0.1 M Tris/HEPES, pH 7.5–8.5, and 25% PEG3350. Pyramidal-shaped crystals were also obtained from 25% PEG1500 as the precipitant solution. Crystals were transferred to a cryoprotectant solution (composed of a higher concentration of mother liquor) for a short period (10–30 s) prior to freezing. The halide derivative of PfDTD crystals was prepared by soaking native crystals for 10–30 s in cryoprotectant solution containing 0.2–1 M sodium iodide. PfDTD-ADP complex crystals were obtained by soaking the native crystals for 10–30 min in cryoprotectant solution containing 5 mM ATP. PfDTD-D-amino acid complex crystals were obtained by soaking crystals from 12 to 60 h in cryoprotectant solution containing 5–20 mM of various D-amino acids individually. Native, PfDTD-iodide, and PfDTD-D-

amino acid complex data sets were collected at 100 K using CuKα radiation (λ = 1.54 Å) generated by a Rigaku MicroMax007 rotating anode x-ray generator operated at 40 kV and 20 mA with VariMax HR mirrors. Diffraction images were recorded using a MAR345dtb image plate detector. PfDTD-ADP complex data were collected on a MARCCD detector at the beamline BM14 of the European Synchrotron Radiation Facility. Data were processed using HKL2000 (14). Data collection and processing statistics are summarized in supplemental Table S1.

Structure Determination and Refinement—The crystal structure of PfDTD was determined using iodide-single wavelength anomalous diffraction phasing technique as implemented in PHENIX (15). One refined PfDTD-iodide dimer was subsequently used to determine the native PfDTD, PfDTD-ADP, and PfDTD-D-amino acid complex structures by molecular replacement method using programs Molrep (16) and Auto-Rickshaw (17). All model refinements were carried out using CNS (18) and REFMAC (19). Visual inspection and model building were carried out using the graphics program COOT (20). Crystallographic refinement statistics are given in supplemental Table S1. PROCHECK (21) was used to validate the stereochemical quality of the final models. Structural superimpositions, sequence alignments, and figures were generated using CHIMERA (22) and PyMOL.

In Silico Screening of PfDTD Inhibitors—Molecular docking and *in silico* screening were carried out for the high resolution PfDTD dimer molecule using the docking program FlexX in the Tripos Sybyl 7.7 suite (Tripos, St. Louis, MO) and the NCI diversity library, which contains ~2000 compounds. Lead compounds were selected based on docking score, energy, and hydrogen bond interactions.

Parasite Growth Inhibition Assays—To assess the effect of selected inhibitors on malaria parasite growth *in vitro*, sorbitol-synchronized 3D7 strain *P. falciparum* parasites were cultured in a 96-well plate with varying amounts of different inhibitors for 48 h starting from the ring stage. The culture medium was then changed every day maintaining an appropriate concentration of inhibitor. Parasitemia was counted by fluorescence assay as described earlier (23). After 48 h of growth, 100 μl of SYBR Green I in lysis buffer (0.2 μl of SYBR Green I ml^{-1} of lysis buffer) was added to each well, and the contents were mixed until no visible erythrocyte sediment remained. After 1 h of incubation in the dark at room temperature, fluorescence was measured with a Cytofluor II fluorescence multiwell plate reader from PerSeptive Biosystems (Framingham, Mass) with excitation and emission wavelength bands centered at 485 and 530 nm, respectively, and a gain setting of 50. By using the accompanying Cytofluor software, background reading for an empty well was subtracted to yield fluorescence counts for analysis. Inhibitory concentrations of all lead compounds were then compared and subtracted with chloroquine IC_{50} in parasite cultures. To assess the effect of D-amino acids on malaria parasite growth, synchronized 3D7 strain *P. falciparum* parasites were cultured in the presence of varying concentrations (2, 5, and 10 mM) of D-amino acids. The parasite cultures were also carried out with and without inhibitor compounds at ring stage. Giemsa-stained smears of malaria parasite were made after 48 h of growth and counted under light microscope. Each experiment was repeated thrice.

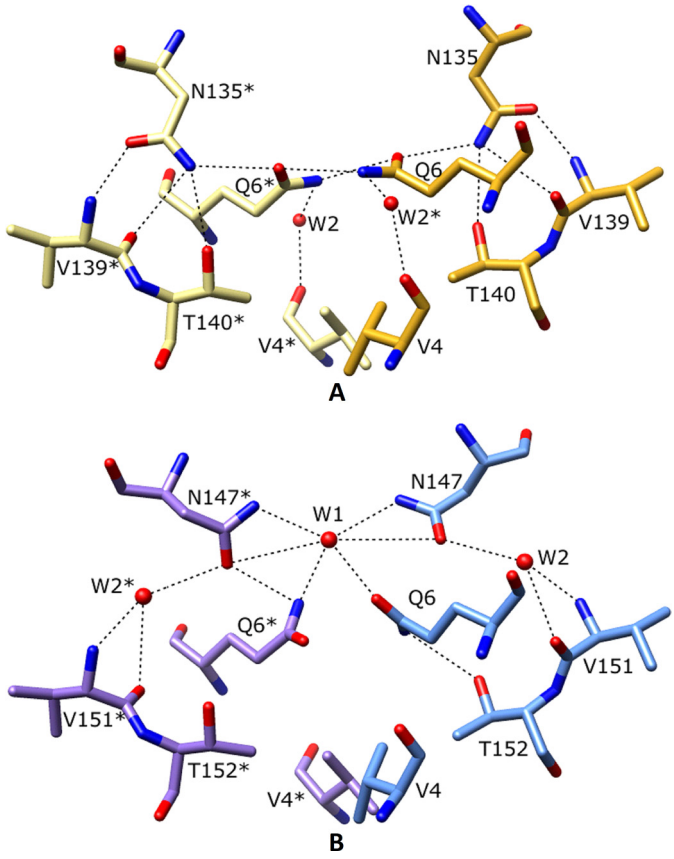

FIGURE 4. **Dimer interface.** *A*, native DTD. The 2-fold-related molecule is labeled with an *asterisk symbol*. *B*, dimer interface of ADP-bound PfDTD structure. Asn-147 adopts different orientations, and an additional water molecule W1 is observed at the dimeric interface.

RESULTS

Deacylase Assay with P. falciparum DTD—The overexpressed and purified PfDTD enzyme-catalyzed D-Tyr-$tRNA^{Tyr}$ hydrolysis at an initial rate of 0.11 ± 0.01 s^{-1}. When L-Tyr-$tRNA^{Tyr}$ was assayed as a substrate under identical conditions, no hydrolysis could be observed. To detect L-Tyr-$tRNA^{Tyr}$ hydrolysis, the enzyme concentration in the assay had to be increased up to 400 nM. At this concentration, the [E] ≪ [S] condition was no more fulfilled. However, we verified that the extent of substrate hydrolysis remained proportional to the enzyme concentration in the assay. A rate of hydrolysis (v = [P]/[E]) of the order of 0.2 ± 0.1 × 10^{-3} s^{-1} could be derived from the experiments with L-Tyr-$tRNA^{Tyr}$. Altogether, these results clearly indicate that PfDTD specifically catalyzes the hydrolysis of D-Tyr-$tRNA^{Tyr}$ (Fig. 1*B*). The specific activity of wild-type PfDTD was determined and compared with the single mutant of S87A (remained active) or double mutants of S87A and T90A (inactive). The double mutant (S87A, T90A) of PfDTD was significantly less active than wild type (data not shown), thus implicating Thr-90 as the reactive residue for catalysis in PfDTD, in line with previous reports suggesting the same (11, 12).

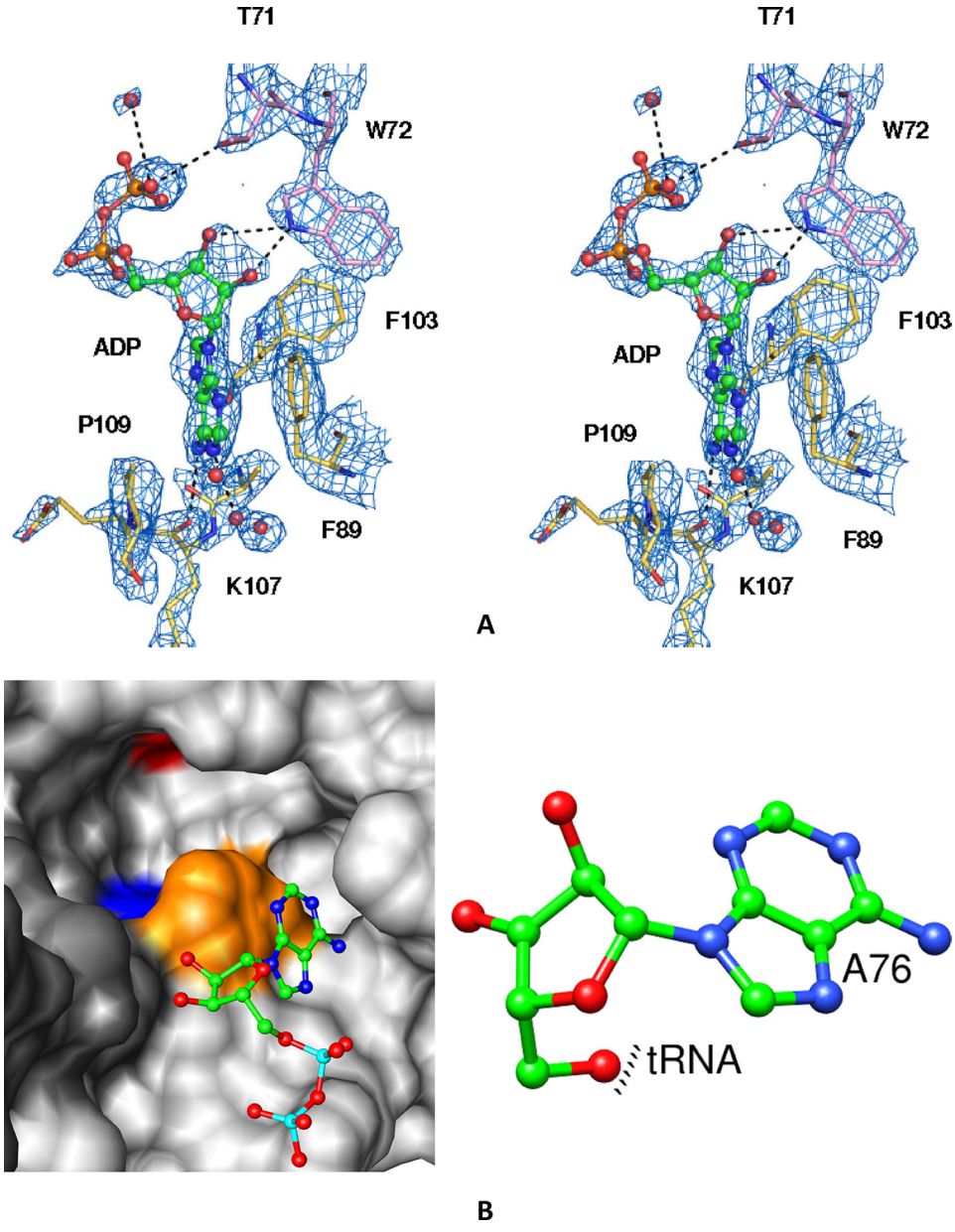

FIGURE 5. **Omit electron density map and surface representation of bound ADP in PfDTD-ATP complex I.** *A*, omit map is contoured at the 1.5σ level near the active site residues in the PfDTD-ATP complex I structure. *B*, surface representation of the PfDTD active site, and bound ADP molecules are shown as a *ball-and-stick model*. The *right side panel* represents the 3′-end of tRNA. Active site residues Phe-89, Thr-90, and Met-141 are shown in *orange*, *blue*, and *red*, respectively.

Subcellular Localization of PfDTD—To test the localization of PfDTD, antibodies were raised in mice against the purified protein. Antibodies were used along with anti-PfNapL antibodies in parasitized red blood cells. The fixed cells were probed with anti-PfDTD and anti-PfNapL antibodies along with DAPI staining (Fig. 1*C*). Results clearly show the co-localization of PfDTD with PfNapL at all the asexual life stages of parasite, suggesting PfDTD to be cytoplasmic in nature, like for PfNapL (24). A signal for PfDTD was also seen at the nuclear periphery with a slight overlap with DAPI, in agreement with previously reported perinuclear localization of human DTD (8).

Description of PfDTD—Triclinic unit cell of PfDTD crystals contains three independent dimeric PfDTDs. PfDTD folds into a compact domain of α/β class of proteins and consists of twisted five-stranded mixed β-sheets covered by two parallel α-helices, three-stranded anti-parallel β-sheets, and two long loops (loop L1, residues 62–81 and loop L2, residues 88–109) (Fig. 2*A*). PfDTD is a 2-fold related dimer and displays extensive dimeric contacts with a buried interface area of ~1200 Å^2. Dimeric interactions are mainly between strand β7 residues, and result in the formation of continuous six-stranded anti-parallel β-sheets. Part of the long loop L2 is also involved in dimeric interactions, which extends from one subunit to the other subunit. Apart from the interactions between strands β7, there are several key hydrogen bonds at the dimer interface: (i) side chain atoms of Gln-88 interact with main chain atoms of Pro-150 and Thr-152, (ii) side chain atom of Thr-90 interacts with main chain atoms of Thr-152, (iii) main chain atoms of Arg-63 interact with main chain atoms of Asn-99, and (iv) side chain atoms of Gln-6 interact with their 2-fold related counterpart. The conformations of the three dimeric PfDTDs in the unit cell are identical except for small yet key differences, including those in the loop regions. The two long loops L1 and L2 show high mobility, and these protrude out of the protein core. Two of six molecules (monomers) in the unit cell have higher B-values (indicative of mobility) than others. Interestingly, *P. falciparum* proteins are often characterized by low complexity loop insertions when compared with their homologs (25). In the case of PfDTD, the low complexity insertion loop IL (residues 17–26) was not evident in the electron density map in most monomers, again suggesting a high degree of flexibility. However, this loop IL was well ordered in a few PfDTD monomers within the unit cell of native and D-amino acid-bound structures (Fig. 2*B*). The IL loop forms an extended β-hairpin structure and makes no contacts with other parts of the PfDTD structure. It is ordered due to lattice contacts only, and we believe that IL which has the sequence KENIGENEKE, represents one of the few views of low complexity insertions that are in abundance in *P. falciparum* proteins (25).

The PfDTD surface has positive charge character around the active site region (Fig. 2*C*). Residues Cys-39 and Cys-59 are proximal, but the electron density maps clearly show that the sulfur atoms do not form a disulfide linkage (Fig. 2*D*). The distance between S-S is ~3.5–3.8 Å, and these distances are comparable with reduced thiols (3.7 Å). These two Cys residues are located in the buried hydrophobic core part of PfDTD. In most DTDs, these two Cys positions are not conserved and are replaced by hydrophobic residues Val/Ile (Fig. 3*A*).

Comparison with Known DTDs: Dimer Interfaces and Active Sites—The PfDTD fold is very similar to its counterparts (AaDTD, EcDTD, HiDTD, and LmDTD, Dali score range of 17–24 with 16–42% sequence identity, r.m.s.d. ~1.1–1.9 Å, Fig. 3, *A* and *B*). PfDTD has a high Dali score of ~25 with HsDTD (r.m.s.d. of 0.9 Å for 148 C^{α} pairs; 45% sequence identity) and of ~15 with the N-terminal editing domain of Thr-tRNA synthetase (called Pab-NTD, 26, 27) (r.m.s.d. 1.9 Å for 114 C^{α} pairs; 16% sequence identity). Among ~50 residues located at dimer interface of DTDs ~50% are conserved (Fig. 3, *A* and *C*). From structure-based sequence alignment, it is clear that conservation among DTDs is highest for dimeric interface residues, possibly linking function with dimeric assembly. In DTDs, the active site is believed to be formed by two highly conserved motifs: residues 87–91 (SQFTL) (Ser-87 is replaced by Pro at times) and 147–152 [N*X*GP(V/F)T] (10–12). The motif SQFTL is at the protein surface, forms an accessible cavity, and links to the NDGPVT motif from the other monomer. The latter motif is mainly involved in dimeric interactions. The DTD active site cavity is surrounded with hydrophobic residues including Phe-89, Phe-103, and Phe-137. The conserved, positively charged residues Arg/Lys-100, Lys-97, Arg-7*, Arg/Lys-58*, and Arg/Lys-63* (2-fold related residues are shown with *) are proximal to the active site, and these may contribute in making electrostatic interactions with tRNA.

The core part of the DTD dimer interface is formed in part due to direct or water-mediated interactions between 2-fold-related Gln-6 from each monomer. However, in the case of PfDTD-ADP complex and LmDTD structures, an additional water (W1) molecule is located near the dimer interface residue Gln-6 (Fig. 4*A*). In PfDTD, the dimer interface residue Asn-147 adopts different conformations when compared with corresponding residues in other DTDs (except in LmDTD where this residue is replaced by Ser) (Fig. 4*B*). In PfDTD, the conformation of Asn-147 residue is controlled by neighboring hydrophobic residues Ile-143 and Val-145, whereas in other DTDs, Ile-143 and Val-145 are replaced by Val and Leu/Ile, respectively (Fig. 3*A*). In HsDTD (12), a Mg^{2+} is located in place of the second water W2 position we have described.

PfDTD Active Site with Bound Adenosine—PfDTD crystals were soaked in 5 mM ATP for 10–30 min, and then diffraction data were collected on these crystals. Strong and clear electron density (for ADP) was observed close to the active site Phe-89, and the electron density maps allowed us to unequivocally model ADP in various PfDTD monomers in PfDTD-ATP complex I (Fig. 5), in PfDTD-ATP complex II, and in PfDTD-ATP complex III structures (supplemental Fig. S1). Binding of ADP appears to be stabilized by a number of interactions with PfDTD. The active site Phe-89 is positioned adjacent to the adenine ring with a stacking distance of ~3.5–4 Å. The other side of the adenine ring is partially in the hydrophobic pocket created by Ala-106 and Pro-109. The ribose hydroxyl groups form hydrogen bonds with side chains of Thr-71 and Trp-72. Amino group N6 of adenine forms a hydrogen bond with main-chain O atom of Lys-107. The phosphate tail of ADP protrudes from the adenine-binding pocket onto the protein surface and adopts variable orientations. The α- and γ-phosphate groups are contacted by a number of direct or water-mediated hydrogen bonds with residues including His-104, Arg-16, Asn-69, and Asp-68. In native and ADP-bound PfDTDs, up to five waters can be found in the active site including the catalytic water Wa1. Waters are also found between Phe-89 and Phe-137, in the active site upper rim region (residues 135–141) and near Tyr-116. In molecule B of PfDTD-ATP complex II structure, we found partially occupied adenine along with five additional waters in the active site region (Fig. 6). Thus, a total of ten waters (including the catalytic Wa1) participate in an elaborate hydrogen-bonding network, which strikingly differs between ADP-bound and native PfDTD. Finally, in molecule B of the PfDTD-ATP complex II, we found the catalytic water Wa1 displaced by ~4 Å from the active site along with an alternate conformation of the active site pocket residue Gln-88. These observations imply crucial roles for waters in ligand-bound and -unbound states of the PfDTD enzyme and have implications in the proposed catalytic mechanism detailed later.

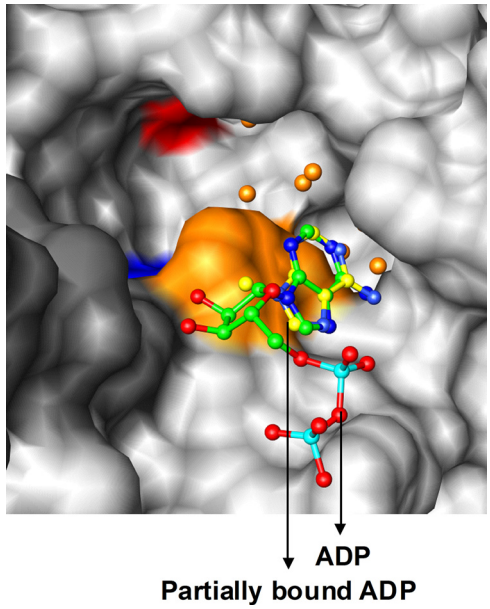

FIGURE 6. **Additional water molecules in the PfDTD active site.** Superimposition of active sites of molecules A and B of the PfDTD-ADP complex II structure. In molecule B, the active site is occupied by partially bound adenine ring (*yellow*), and there are five additional water molecules (*orange spheres*) between the adenine entry point and the enantio-selectivity checkpoint. Active site residues are colored as described in the legend to Fig. 5.

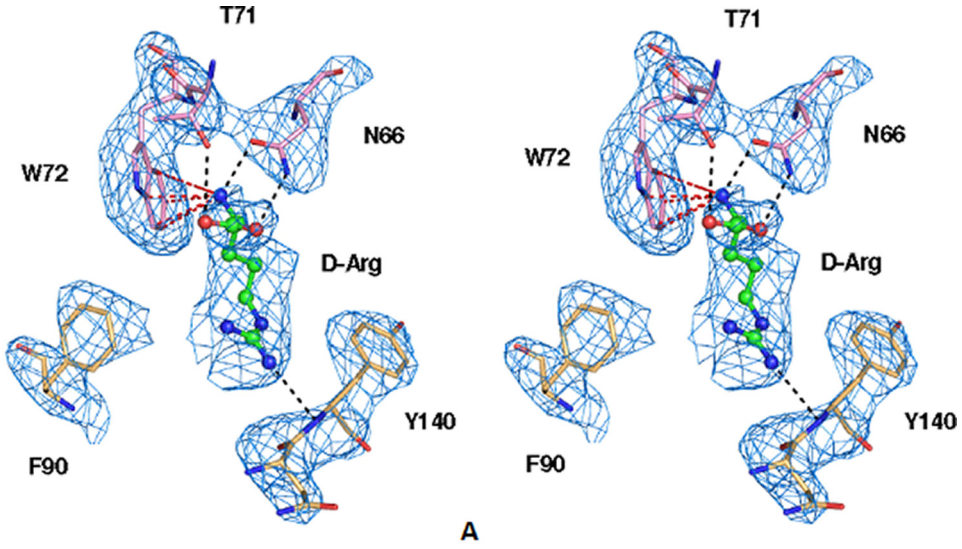

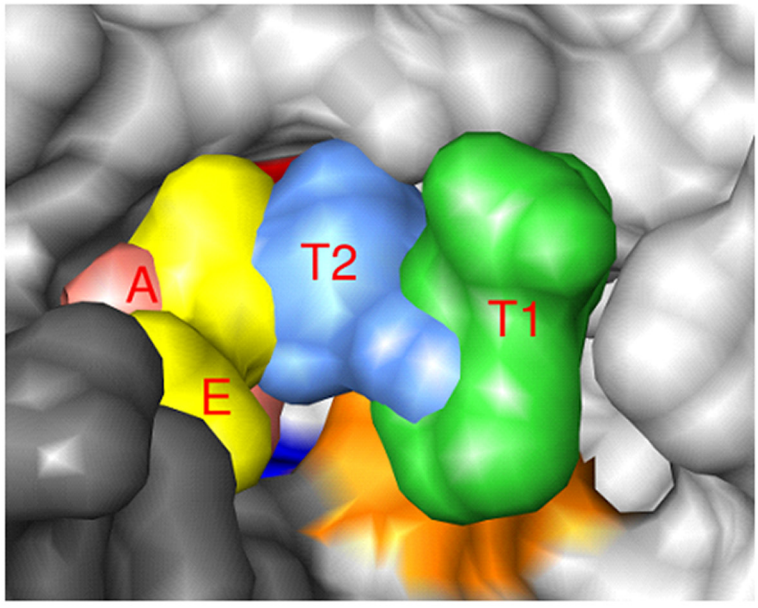

FIGURE 7. **Omit electron density map near the active site in PfDTD-D-Arg complex and subsite classifications of bound D-amino acids.** *A*, omit map is contoured at the 1.5 σ level around the active site residues. Hydrogen bonds and N-H…π are marked with *black* and *red dashed lines*, respectively. *B*, bound D-amino acids in PfDTD cluster at four different subsites within the active pocket, and we have termed these sites as transition subsites (T1 and T2), active subsite A, and exit subsite E.

D-Amino Acid Subsites in PfDTD—D-Amino acid specificity in PfDTDs was investigated based on crystals structures of PfDTD complexed with various D-amino acids. Native PfDTD crystals were soaked in D-amino acids, and then diffraction data were collected on these crystals. For each complex, difference Fourier electron density and omit maps revealed docking of D-amino acids near the active site pocket. We soaked in D-Arg, D-Lys, D-Glu, D-Ser, and D-His in these studies, and we observed clear electron density for these D-amino acids (Fig. 7*A* and supplemental Fig. S2). In the case of the D-His complex, one of the bound D-His is located near the active site Phe-89, and its side chain is involved in edge-to-face π…π interaction with the active site Phe-89. The other D-His is located near the upper rim of the active site loop where the potentially enantio-selective Met-141 residue sites (see below). The amino group of this latter D-His interacts with main-chain carbonyl oxygen atoms of Gly-138 and Asn-139. The bound D-Ser is found at two different places within the active site cavity. Finally, the negatively charged D-Glu and the positively charged D-Arg and D-Lys were found near the active Thr-90. The carboxyl oxygen atoms of D-Glu form one hydrogen bond with Asn-66 and make a salt-bridge interaction with Arg-7. D-Arg and D-Lys make similar interactions with protein atoms by means of their α-amino and carboxyl groups. Their electropositive α-amino group is stabilized by N-H…π interaction with the benzene ring of Trp-72 and $O^{\delta 1}$ of Asn-66. The carboxyl group of D- Arg and D-Lys also interacts with $N^{\delta 2}$ of Asn-66. As shown in Figs. 7*B* and 8, the bound D-amino acids cluster at four different subsites within the PfDTD active site pocket, and we have termed these sites as transition subsites (T1 and T2), active subsite (A), and exit subsite (E). T1 and T2 are the transition subsites where initial recognition and positioning of D-amino acids take place. Chiral selection most likely takes place at the T2 subsite by the residue Met-141. The breakdown of the ester bond between D-amino acid and tRNA likely occurs at the active subsite A where Thr-90 resides. The subsite E likely represents the post-transfer state of the deacylation reaction where cleaved D-residues are dumped for subsequent diffusion away from PfDTD. In the five PfDTD-D-amino acid complex structures we have studied, we found two (D-His and D-Ser) in the subsite T1 and D-His in T2. We could also locate another two (D-Glu and D-Ser) proximal to the active subsite A, and the last two (D-Arg and D-Lys) were identified at subsite E (Fig. 8).

Active Site Comparison of PfDTD with Pab-NTD and Subsite Classifications—PfDTD and Pab-NTD have similar folds, but these two enzymes differ in amino acid enantio-selectivity (26, 27). DTD is specific to D-aa-tRNA and not to L-aa-tRNA, whereas Pab-NTD is specific for L-ser-$tRNA^{Thr}$ among others. We have superimposed the crystal structure of Pab-NTD complex with pre-transfer (seryl-3′-aminoadenosine,

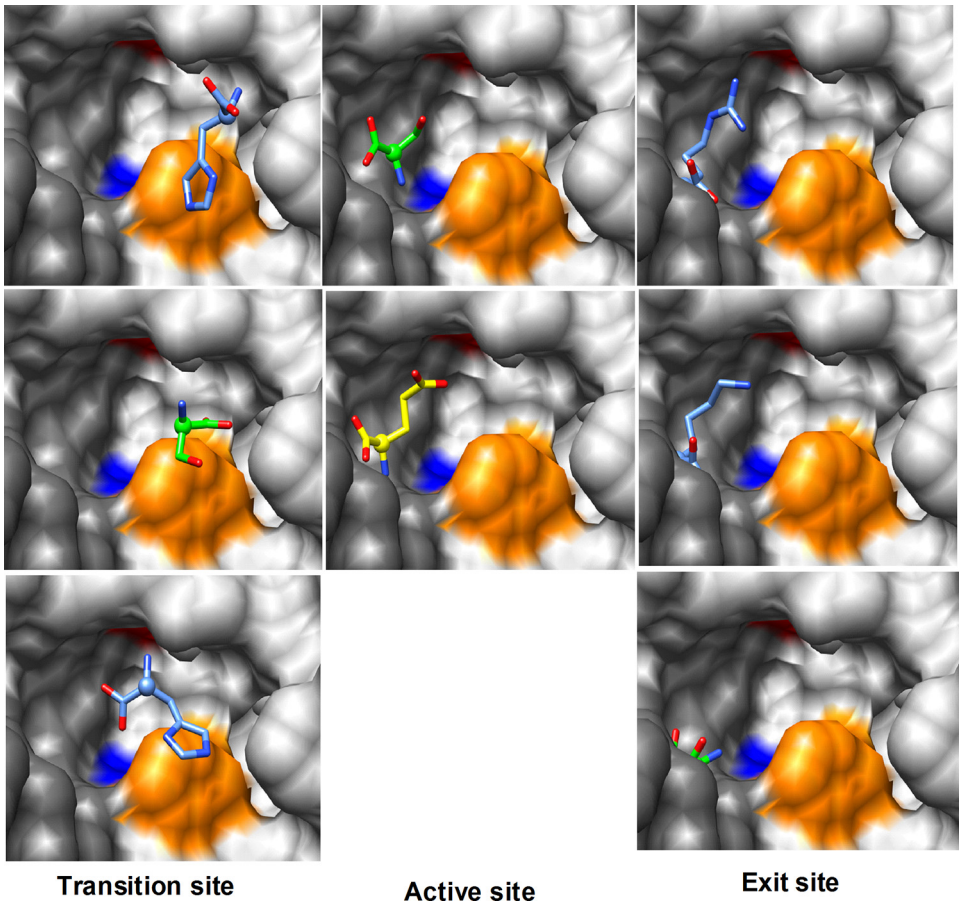

FIGURE 8. **Surface representation of bound D-amino acids in various subsites.** D-amino acids (*ball-and-stick*) located in different subsites (T1, T2, A, and E) within the active site pocket of PfDTD. Active site residues are colored as in Fig. 5.

A3S) analog on to ADP-bound PfDTD (Fig. 9*A*). These structural comparisons have been very revealing. The bound adenine ring in PfDTD and Pab-NTD complex structures do not coincide, as the ADP in PfDTD is located near the entry point of the active channel. In contrast, in Pab-NTD, the adenine ring of A3S analogs is found deeper in the active site cleft, a region where we found five water molecules in molecule B of the PfDTD-ATP complex II structure. The invariant residues Val-45, Ala-94, and Phe-117 of Pab-NTD in the adenine-binding pocket are replaced by corresponding conserved residues Ile/Val-43, Ala-112, and Phe-137 in other DTDs. However, the two key DTD active site motifs [SQFTL and N*X*GP(V/F)T] are not conserved in Pab-NTD and therefore several important differences are to be expected in the adenine recognition. In PfDTD, Ser-87 (of motif SQFTL) interacts with N3 of the bound adenine. When Pab-NTD is superimposed on PfDTD, it is evident that the L-Ser of A3S is resident in our defined subsite T2, close to the chiral checkpoint residue Met-141 of PfDTD. This placement is in proximity to the crucial Met-141, which potentially serves as the enantiomeric selectivity checkpoint, based on mutagenesis studies (26, 27). In these previous experiments, the D/L-amino acid binding affinities were studied based on fluorescence binding assays for wild-type and single mutant of EcDTD (Met-129 to Lys) and Pab-NTD (Lys-121 to Met). DTDs are specific for D-amino acids (D-aa-tRNA), whereas Pab-NTD is specific for only L-Ser-tRNA^{Thr}. However, the M129K mutant of EcDTD was shown to bind L-amino acids, whereas the K121M mutant of Pab-NTD showed deacylation activity thus assigning enantio-selectivity role to the conserved methionine in DTDs (26, 27).

Based on bound ADP molecules in PfDTD and substrate analogues in Pab-NTD, we propose that recognition and docking of the terminal adenine of D-aa-tRNA involves two spatial regions, termed as transition subsites B1 and B2 (Fig. 9*B*). In PfDTD-D-amino acid complex structures, we found various D-amino acids at different positions of the active site (Fig. 8). Taken together, we have classified the active site pockets within PfDTD as B1, B2 for adenosine positions and as T1, T2, A, and E for the various D-amino acid positions. These spatial sectors within PfDTD allow a complete explanation of the catalytic cycle (Fig. 9*C*). The conserved Met-141 side chain points toward the bottom of the A subsite. Interestingly, in all representations of DTDs, and specifically in the multiple copies of PfDTDs we have solved here, the conserved Met-141 always adopts an invariant conformation. This observation suggests that this key residue may provide chiral selectivity property to DTDs (26, 27). Further, the buried Met-141 is chaperoned by highly conserved hydrophobic residues, Pro-150, Val-86, Phe-40, Val-15, Leu-13, and Gly-135. Additionally, conserved residues Phe-137 and Tyr-116 are located at bottom of subsite T2. When we compared all DTDs, we observed flipping of the main chain carbonyl groups of Phe-137 and Gly-135. We also noticed movement of Ser-87, Gln-88, Phe-137, and Tyr-116 side chains (supplemental Fig. S3). These small perturbations possibly indicate flexibility at the bottom of the active site region and may reflect closing and opening of the active site lid. The active site Thr-90 is shielded from solvent by Phe-89, which adopts similar conformations in most DTD structures, we believe these represent tRNA-bound open conformations of Phe-89 in the active site (*i.e.* subsites B1 and B2) (Fig. 10*A*). In contrast, closed conformations are represented by some structures (HiDTD, one case of EcDTD-molecule D and by HsDTD-molecule C, Fig. 10*B*). In these closed DTDs, Phe-89 (or its equivalent) adopts shut conformations thereby disallowing docking of terminal adenine of charged tRNA onto DTD.

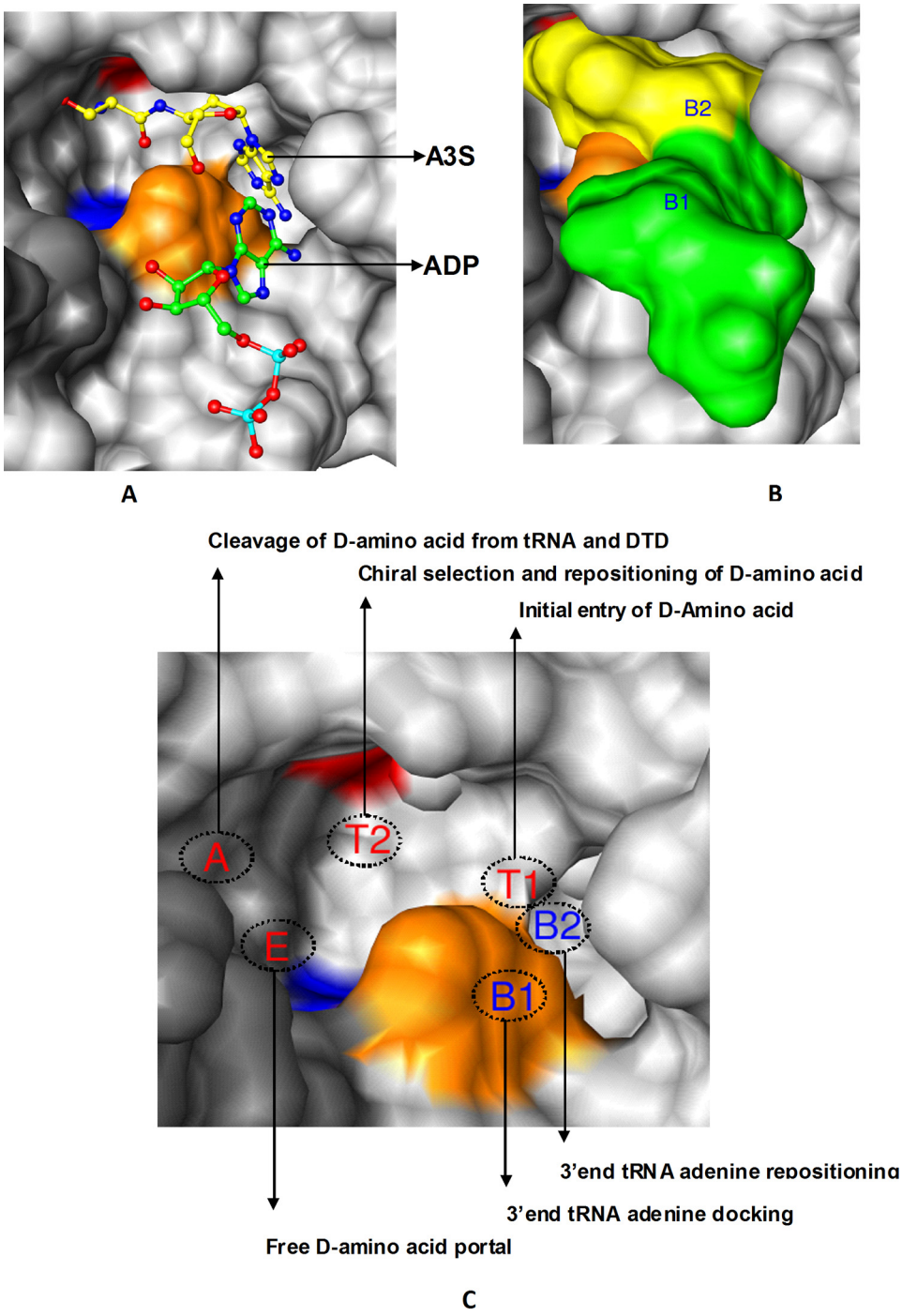

FIGURE 9. **Views of the PfDTD-ADP structure with the substrate analog of Pab-NTD along with PfDTD subsites.** *A*, superimposition of pre-transfer substrate analog (seryl-3′-aminoadenosine, A3S, *yellow*) complex structure of Pab-NTD onto ADP-bound PfDTD. *B*, bound adenine ring in PfDTD and in Pab-NTD complexes mimics entry point of tRNA. We termed these subsites as transition sites B1 and B2, respectively. *C*, classification of various subsites in the active site pocket of DTDs. Active site residues are colored as in Fig. 5.

Docking of D-Tyr-tRNA into PfDTD Active Site—Based on the above insights, we built a model for the 3′-end of D-Tyr-tRNA substrate analog (tyrosyl-3′-aminoadenosine, A3Y, Fig. 11*A*) at the PfDTD active site. We mutated (*in silico*) the L-ser of A3S (Pab-NTD) to D-Tyr and considered its placement in subsite A of PfDTD. This modeling made it immediately apparent that the D-Tyr was now ideally placed for chirality selection near Met-141 (subsite T2) at a distance of 2.5–3.0 Å and without steric clashes (Fig. 11*B*). This resulted in a distance of ~5 Å between the D-Tyr carboxyl carbon atom and the active site Thr-90 hydroxyl group. Based on observed PfDTD conformations in our structures, we then modeled side chain conformations of Gln-88, Phe-89, and of the active residue Thr-90 toward the D-Tyr carbonyl carbon atom. The above described minor adjustments allow the D-Tyr carbonyl carbon to point directly toward the hydroxyl group of the active site residue Thr-90, ready for catalysis.

A Model for Catalytic Mechanism—A comprehensive scheme for catalytic mechanism of DTDs, which involve cleavage of ester bond between D-Tyr/tRNA and of D-Tyr/DTD, can now be proposed based on our studies (Fig. 12). In this family of enzymes, catalysis is a substrate-assisted two step process. In the first step, the side chain O^{γ} of Thr-90 attacks the D-amino acid carbonyl carbon (C′) in a nucleophilic manner and also deprotonates the α-amino group of D-amino acid (Fig. 12*A*). This leads to formation of tetrahedral transition state, which is stabilized by the oxyanion hole formed by main-chain N atoms of Phe-89 and Thr-90 as well as by the side chain $N^{\epsilon 2}$ of Gln-88. This is followed by cleavage of the D-amino acid-tRNA ester bond. The uncharged tRNA then moves out of the active site for diffusion into the solution whereas the D-amino acid remains bound to the DTD enzyme. Subsequently, the ester bond between DTD and the D-amino acid is cleaved by the catalytic water molecule Wa1, leading to removal of the cleaved free D-amino acid from subsite A and its placement into the exit subsite E (Fig. 12, *B* and *C*). These events thus complete catalytic cycle of deacylation and lead to generation of both free tRNA and D-amino acids.

In Silico Screening and Parasite Growth Inhibition Assays—Based on the docking scores, energy values, and hydrogen-bonding interactions, several PfDTD-inhibitor complex structures (*in silico*) were short-listed, and the top 40 compounds were selected for testing in parasite growth inhibition assays.

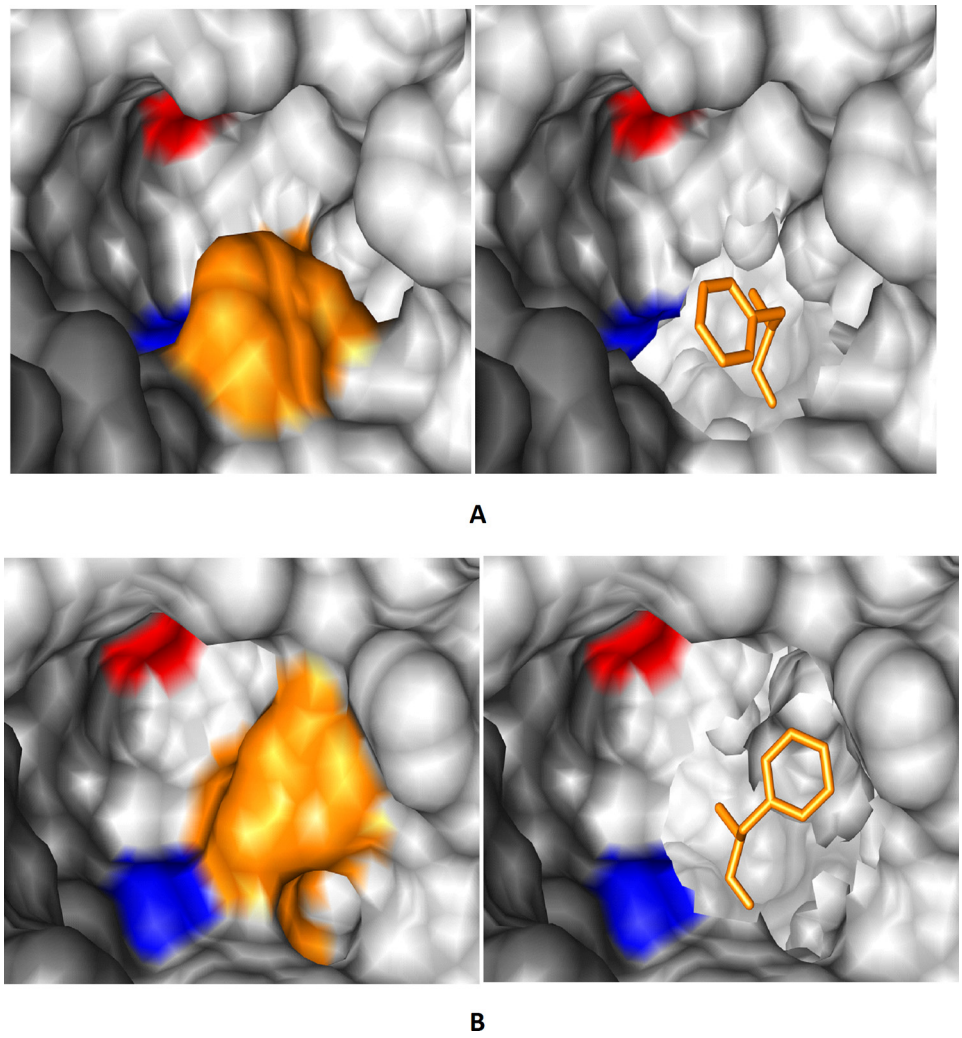

FIGURE 10. **Surface representation of open and close conformations of Phe-89 at the adenosine-docking site.** *A*, open conformation of active site Phe-89 in native DTDs, in D-amino acid-bound and ADP-bound structures. The stick model of Phe-89 is shown in the *right side panel*. Color codes of active site residues are as in Fig. 5. *B*, closed conformation of Phe-89 is observed in HiDTD, molecule D of EcDTD, and molecule C of HsDTD.

Synchronized parasite cultures at ring stages were incubated with inhibitors at varying concentrations ranging from 10 nM to 100 μM. Out of 40 selected compounds, four compounds showed inhibition of parasite growth (Fig. 13*A*). At the 10 μM concentration, compound 2 [*N,N′-bis(4-amino-2-methyl-6-quinolinyl)urea*] showed more than 90% inhibition of parasite growth. Further, parasites were grown in varying concentrations of D-isoleucine either in the presence or absence of 0.1 μM concentration of compound 2. The data suggest that addition of compound 2 likely makes parasite sensitive to higher concentrations of D-isoleucine (Fig. 13*B*), suggesting inhibition of PfDTD by compound 2, possibly by disabling detoxification of D-isoleucine by the parasite.

DISCUSSION

PfDTD was overexpressed in *E. coli*,, and the recombinant purified protein was crystallized in three different crystal growth solutions. We determined PfDTD structure using iodide-SAD technique, and we subsequently solved three different PfDTD-ADP structures along with several PfDTD-D-amino acid complex structures. The PfDTD crystals belong to a triclinic unit cell with three dimers each in the asymmetric unit. This presented PfDTD-ligand structures with three independent atomic views of the dimers. Further, the ligand-soaked crystals diffracted to higher resolution than native crystals facilitating better quality atomic dissection of PfDTD-ligand complexes.

High resolution PfDTD-ligand structures allowed us to map transition/movement of each of the chemical groups involved in the deacylation reaction, including those involving protein side chains, the adenine ring, and the ribose pucker. The bound adenine ring stacks with active site Phe-89 in PfDTD, and this binding marks the transition site B1 that participates in recognition of the 3′-end of charged tRNA. We show that PfDTD bound D-amino acids cluster at three different subsites, termed transition, active, and exit, around and near the active site Thr-90 residue, which initiates catalysis. Our PfDTD co-crystal structures provide glimpses of several reaction intermediates. An in-depth analysis of substrates, products, and water networks has therefore allowed us to make an elaboration of PfDTD active site into multiple spatial components. Previously, catalytic mechanisms for DTDs have been proposed based on modeling studies (11, 12). Our experimental data on PfDTD substrate interactions support the proposed reaction schemes and provide the first structural basis for these mechanisms. We propose several sequential steps that eventually catalyze deacylation of D-aa-tRNAs by DTD. These steps are: (i) electrostatic interactions along with minor conformational changes in PfDTD facilitate docking of 3′-end of tRNA on to PfDTD, (ii) insertion of water W1 at the dimeric interface and side chain movements of Asn-147 and water W2 then create space between PfDTD monomers (Fig. 4). This is followed by tethering of tRNA terminal adenine to entry point/transition site B1 of the active site Phe-89. It also allows for entry of covalently bound D-amino acid into the amino acid transition subsite T1, (iii) because of these steps, the pre-bound waters in the active region escape, making way for authentic substrates to reposition themselves. For example, exit of the pre-bound waters (found in our PfDTD complexes) likely facilitate flipping of carbonyl groups belonging to residues 135/137 and also allow movement of Ser-87 (Fig. 9 and

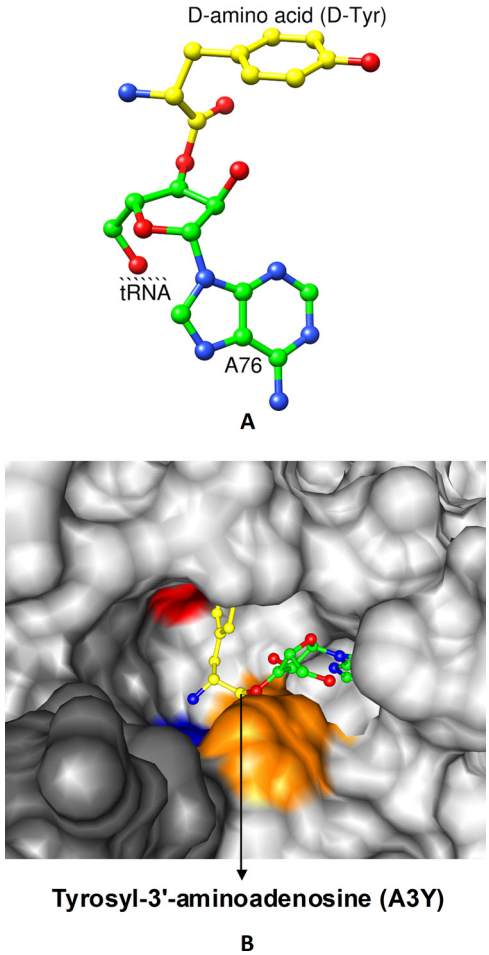

FIGURE 11. **Modeled 3′-end of D-Tyr charged tRNA (tyrosyl-3′-aminoadenosine, A3Y) in the active site of PfDTD.** *A*, *ball-and-stick* representation of A3Y that mimics the 3′-end of D-amino acid (*yellow*)-charged tRNA (*green*). *B*, modeled A3Y at B2 subsite in PfDTD. The position of the carbonyl carbon atom of tyrosyl is near the active Thr-90. Active site residues are colored as in Fig. 5.

supplemental Fig. S3). These minor conformational adjustments structurally and spatially rebuild the PfDTD active site, (iv) the above structural alterations then translate into side chain movements of Tyr-116, Phe-137, Phe-89, and Gln-88. Also, crucially there is a 120° rotation of the active site Thr-90 side chain. These then trigger traversal of D-amino acid-charged tRNA from transition site B1 to B2. Subsequently, the D-amino acid is presented in the enantiomer selectivity pocket (subsite T2). The task of enantiomeric selectivity is then potentially done by the completely invariant, conformationally restrained, and biochemically implicated Met-141 (26, 27). Once the amino acid chirality is acceptable, its carbonyl carbon is placed proximal to the catalytic Thr-90, (vi) in the subsequent catalytic step, side chain O^{γ} of Thr-90 attacks the D-amino acid carbonyl carbon (C′) in a nucleophilic manner and the deprotonated amino group of D-amino acid accepts the hydroxyl proton from Thr-90. Thus, the tetrahedral transition state is formed and cleavage of D-aa-tRNA ester bond can take place (Fig. 11). The uncharged tRNA can thus exit the active site whereas the D-amino acid remains bound to DTD enzyme, vii) in the last step, catalytic water Wa1 moves into the active site and attacks the ester bond between DTD and D-amino acid resulting in its cleavage. The cleaved free D-amino acid subsequently enters the exit subsite E, which we have annotated in PfDTD. These steps represent the catalytic cycle and therefore allow generation of free DTD, free tRNA, and free D-amino acid. In summary, we present direct experimental evidence for the presence of several subsites within DTD, which together enable docking, cleavage, and egress of the recognized D-amino acid, thus leaving uncharged tRNA for another round of the aminoacylation reaction. The co-crystal structures of five D-amino acids with PfDTD also reveal inherent plasticity in the D-amino acid recognition sites. The latter is significant, because PfDTD is required to accommodate and catalyze reactions despite considerable differences in shape, size, and charge of D-amino acids.

Using structure-based *in silico* screening routines, we selected 40 compounds for testing in parasite growth inhibition assays. Out of these, four compounds showed significant inhibition of parasite growth and compound 2 (*N*,*N*′-bis(4-amino-2-methyl-6-quinolinyl)urea, Fig. 13*B*) showed more than 90% inhibition. Compound 2 was found to dock at B1 and B2 subsites of PfDTD active site pocket, where the terminal adenosine of D-amino acid charged tRNA docks during deacylation; this observation implies that compound 2 might be competing with PfDTD substrate. These data provide initial evidence that inhibitors like compound 2 may be useful as novel inhibitors against the malaria parasite given that only a single copy of *dtd* gene is present in the malaria genome. We also observed that higher concentrations of D-isoleucine (L-isoleucine is absent in hemoglobin and therefore presumably it is important for the parasite to import this) in the RPMI medium do not affect growth of malaria parasite. Among others, there could be two possible reasons for this, either D-isoleucine is poorly absorbed by the parasite or the parasite-encoded DTD enzyme neutralizes expected toxicity of D-isoleucine. Our data indicate that the presence of the inhibitory compound 2 in the medium makes parasite growth vulnerable to higher D-isoleucine concentrations (Fig. 13*B*). This observation suggests that active PfDTD may be important for the malaria parasite in terms of overcoming D-amino acid-induced toxicity. Interestingly, compound 2 has been previously tested on J774A.1 cells (macrophage cell line) at up to 100 μM concentration, and it showed negligible cytotoxicity (28).

In conclusion, we present a comprehensive mechanism for the deacylation reaction by the DTD class of proofreading enzymes. Our structural studies suggest how D-amino acid-charged tRNA may be recognized and processed by PfDTD. These studies also provide direct comparisons with the previously characterized Pab-NTD enzyme family. The description of multiple subsites within DTD active site pocket provides a first view of the structural architecture required by these enzymes to perform their editing functions. Our results also suggest that specific inhibitors against PfDTD may hinder parasite growth in the presence of D-amino acids. DTDs from pathogenic organisms like *P. falciparum* can therefore be explored

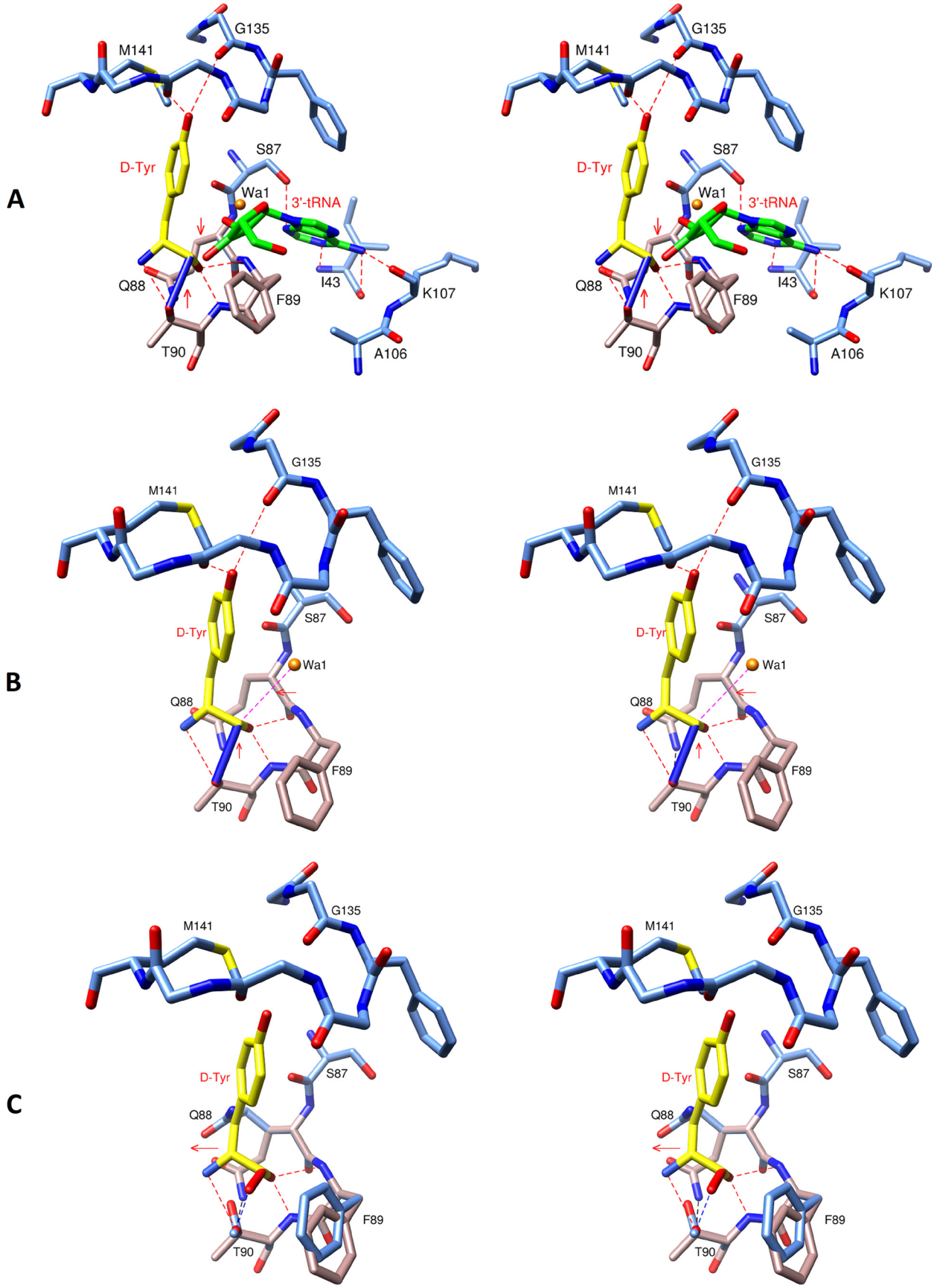

FIGURE 12. **Proposed catalytic mechanism.** *A*, hydroxyl group of Thr-90 attacks carbonyl carbon of A3Y in a nucleophilic manner, followed by cleavage of ester bond and formation of acyl enzyme (D-amino acid bound to DTD). *B*, movement of catalytic water Wa1 close to carbonyl carbon of D-amino acid. *C*, cleavage of ester bond between D-amino acid and DTD. Thus, free D-amino acid may migrate to subsite E from where it could diffuse.

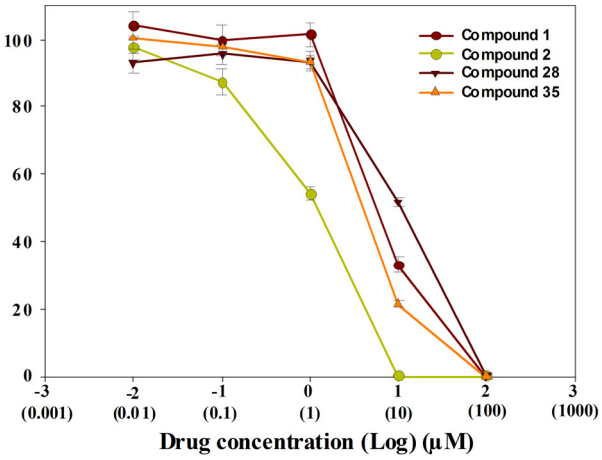

A

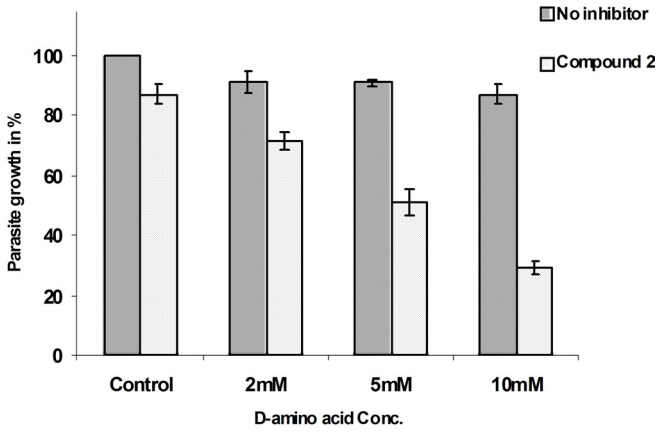

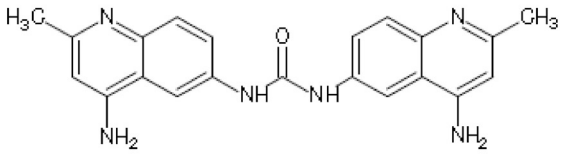

NSC 12155: N,N'-bis(4-amino-2-methyl-6-quinolinyl)urea

B

FIGURE 13. **Parasite inhibition assays.** *A*, growth of cultures of *P. falciparum* after 48 h in the presence of four different inhibitors at varying concentrations ranging from 0.01 to 100 μM. *B*, parasites growth at varying concentrations of D-isoleucine in presence or absence of 0.1 μM concentration of compound 2 in the medium. The structure of compound 2 is shown.

further for their value as novel and unique targets for the focus of antimalarials.

Acknowledgments—We thank Pierre Plateau and Sylvain Blanquet for helping with enzyme activity assays. The X-ray facility at ICGEB, New Delhi, is funded by the Wellcome Trust.

REFERENCES

1. Calendar, R., and Berg, P. (1966) *Biochemistry* **5,** 1681–1690
2. Calendar, R., and Berg, P. (1966) *Biochemistry* **5,** 1690–1695
3. Soutourina, J., Blanquet, S., and Plateau, P. (2000) *J. Biol. Chem.* **275,** 11626–11630
4. Soutourina, J., Plateau, P., and Blanquet, S. (2000) *J. Biol. Chem.* **275,** 32535–32542
5. Soutourina, J., Plateau, P., Delort, F., Peirotes, A., and Blanquet, S. (1999) *J. Biol. Chem.* **274,** 19109–19114
6. Wydau, S., Ferri-Fioni, M. L., Blanquet, S., and Plateau, P. (2007) *Nucleic Acids Res.* **35,** 930–938
7. Ferri-Fioni, M. L., Fromant, M., Bouin, A. P., Aubard, C., Lazennec, C., Plateau, P., and Blanquet, S. (2006) *J. Biol. Chem.* **281,** 27575–27585
8. Zheng, G., Liu, W., Gong, Y., Yang, H., Yin, B., Zhu, J., Xie, Y., Peng, X., Qiang, B., and Yuan, J. (2009) *Biochem. J.* **417,** 85–94
9. Snow, R. W., Guerra, C. A., Noor, A. M., Myint, H. Y., and Hay, S. I. (2005) *Nature* **434,** 214–217
10. Ferri-Fioni, M. L., Schmitt, E., Soutourina, J., Plateau, P., Mechulam, Y., and Blanquet, S. (2001) *J. Biol. Chem.* **276,** 47285–47290
11. Lim, K., Tempczyk, A., Bonander, N., Toedt, J., Howard, A., Eisenstein, E., and Herzberg, O. (2003) *J. Biol. Chem.* **278,** 13496–13502
12. Kemp, M., Bae, B., Yu, J. P., Ghosh, M., Leffak, M., and Nair, S. K. (2007) *J. Biol. Chem.* **282,** 10441–10448
13. Winter, G., Kawai, S., Haeggström, M., Kaneko, O., von Euler, A., Kawazu, S., Palm, D., Fernandez, V., and Wahlgren, M. (2005) *J. Exp. Med.* **201,** 1853–1863
14. Otwinowski, Z., and Minor, W. (1997) *Methods Enzymol.* **276,** 307–326
15. Adams, P. D., Grosse-Kunstleve, R. W., Hung, L. W., Ioerger, T. R., McCoy, A. J., Moriarty, N. W., Read, R. J., Sacchettini, J. C., Sauter, N. K., and Terwilliger, T. C. (2002) *Acta Crystallogr. D Biol. Crystallogr.* **58,** 1948–1954
16. Vagin, A., and Teplyakov, A. (1997) *J. Appl. Crystallogr.* **30,** 1022–1025
17. Panjikar, S., Parthasarathy, V., Lamzin, V. S., Weiss, M. S., and Tucker, P. A. (2005) *Acta Crystallogr. D Biol. Crystallogr.* **61,** 449–457
18. Brünger, A. T., Adams, P. D., Clore, G. M., DeLano, W. L., Gros, P., Grosse-Kunstleve, R. W., Jiang, J. S., Kuszewski, J., Nilges, M., Pannu, N. S., Read, R. J., Rice, L. M., Simonson, T., and Warren, G. L. (1998) *Acta Crystallogr. D Biol. Crystallogr.* **54,** 905–921
19. Murshudov, G. N., Vagin A. A., and Dodson, E. J. (1997) *Acta Crystallogr. D Biol. Crystallogr.* **53,** 240–255
20. Emsley, P., and Cowtan, K. (2004) *Acta Crystallogr. D Biol. Crystallogr.* **60,** 2126–2132
21. Laskowski, R. A., MacArthur, M. W., Moss, D. S., and Thornton, J. M. (1993) *J. Appl. Crystallogr.* **26,** 283–291
22. Pettersen, E. F., Goddard T. D., Huang C. C., Couch, G. S., Greenblatt, D. M., Meng, E. C., and Ferrin, T. E. (2004) *J. Comput. Chem.* **25,** 1605–1612
23. Smilkstein, M., Sriwilaijaroen, N., Kelly, J. X., Wilairat, P., and Riscoe, M. (2004) *Antimicrob. Agents Chemother.* **48,** 1803–1806
24. Chandra, B. R., Olivieri, A., Silvestrini, F., Alano, P., and Sharma, A. (2005) *Mol. Biochem. Parasitol.* **142,** 237–247
25. Singh, G. P., Chandra, B. R., Bhattacharya, A., Akhouri, R. R., Singh, S. K., and Sharma, A. (2004) *Mol. Biochem. Parasitol.* **137,** 307–319
26. Dwivedi, S., Kruparani, S. P., and Sankaranarayanan, R. (2005) *Nat. Struct. Mol. Biol.* **12,** 556–557
27. Hussain, T., Kruparani, S. P., Pal, B., Dock-Bregeon, A. C., Dwivedi, S., Shekar, M. R., Sureshbabu, K., and Sankaranarayanan, R. (2006) *EMBO J.* **25,** 4152–4162
28. Panchal, R. G., Hermone, A. R., Nguyen, T. L., Wong, T. Y., Schwarzenbacher, R., Schmidt, J., Lane, D., McGrath, C., Turk, B. E., Burnett, J., Aman, M. J., Little, S., Sausville, E. A., Zaharevitz, D. W., Cantley, L. C., Liddington, R. C., Gussio, R., and Bavari, S. (2004) *Nat. Struct. Mol. Biol.* **11,** 67–72